CHAPTER 6

Tidal Dynamics of Groundwater Flow and Contaminant Transport in Coastal Aquifers

L. Li, D.A. Barry, D.-S. Jeng, H. Prommer

1. INTRODUCTION

Coastal/estuarine water pollution is becoming an increasingly serious global problem largely due to input of land-derived contaminants. For example, nutrient leachate from the sugar cane production areas of North-East Queensland is causing great concern for the Great Barrier Reef in Australia [Haynes and Michael-Wagner, 2000]. The resulting degradation of coastal resources affects significantly economic and social developments of coastal regions. Traditionally, terrestrial fluxes of chemicals to coastal water have been estimated on the basis of river flow alone. However, recent field observations indicate that contaminants entering coastal seas and estuaries with groundwater discharge (submarine groundwater discharge, SGWD) can significantly contribute to coastal pollution, especially in areas where serious groundwater contamination has occurred (e.g., Moore [1996], Burnett *et al.* [2001]). The International Geosphere-Biosphere Programme (IGBP) [Buddemeier, 1996] has identified submarine groundwater discharge as an important but rather unknown source of contamination for coastal marine and estuarine environments. As the groundwater contamination problem worsens, the SGWD may become a dominant source of coastal pollution in certain areas.

SGWD consists of both groundwater flow from upland regions and water exchange at the aquifer–ocean interface [Simmons, 1992]. While the upland groundwater flow can be estimated based on the aquifer recharge [Zekster and Loaiciga, 1993], it is difficult to quantify the rate of water exchange across the seabed, which is influenced by near-shore processes [Li *et al.*, 1997a; Turner *et al.*, 1997; Li and Barry, 2000]. Large rates of SGWD, derived from geochemical signals of enriched natural tracers (e.g., ^{226}Ra) [Moore, 1996] in coastal seas, have been found excessive and cannot

1-56670-605-X/04/$0.00+$1.50

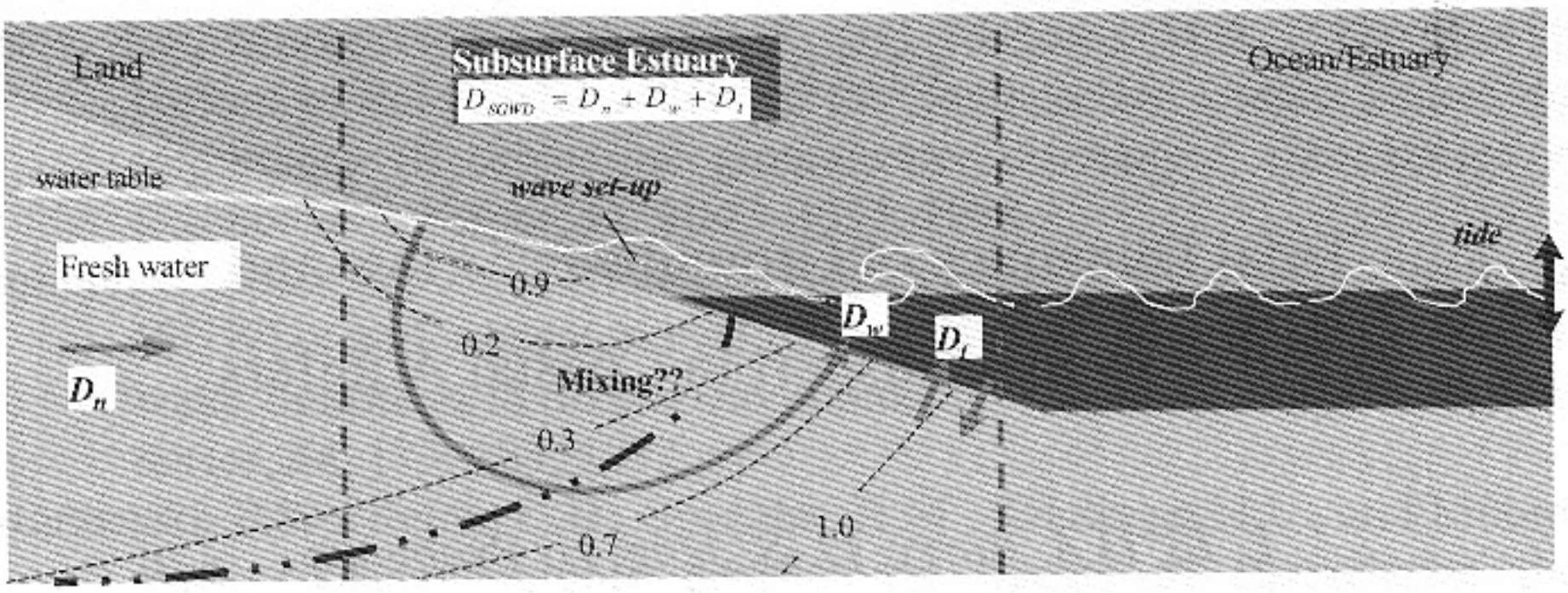

Figure 1: A simple model of SGWD consisting of inland fresh groundwater flow (D_n) and seawater recycling (water exchange due to wave set-up D_w, and due to tides D_t). The mixing of the recycling water with fresh groundwater results in the near-shore salinity profiles as schematically shown by the thin dashed lines (in contrast with the traditional saltwater wedge view shown by the thick dot-dashed line).

be supported by the aquifer recharge [Younger, 1996]. This suggests that water exchange at the interface may have constituted a large portion of the SGWD. A theoretical model of SGWD has been developed to include tidally oscillating groundwater flow and circulation due to wave set-up (i.e., on-shore tilt of the mean sea level; Figure 1). These two local processes were found to cause a large amount of water exchange across the interface.

Although the exchanging/recycling water is largely of marine origin, it mixes and reacts with groundwater and aquifer sediments, modifying the composition of the discharging water. The exchange processes can reduce the residence time of chemicals in the mixing zone of the aquifer, similar to tidal flushing of a surface estuary [Li *et al.*, 1999]. As a result, the rates of chemical fluxes from the aquifer to the ocean increase but the exit chemical concentrations are reduced (dilution effects). The exchange can also alter the geochemical conditions (redox state) in the aquifer and affect the chemical reactions. It has been shown numerically that the exchange enhances the mixing of oxygen-rich seawater and groundwater, and creates an active zone for aerobic bacterial populations in the near-shore aquifer. This zone leads to a considerable reduction in breakthrough concentrations of aerobic biodegradable contaminants at the aquifer–ocean interface [Enot *et al.*, 2001; Li *et al.*, 2001].

In essence, the water exchange and subsequent mixing of the recycling water with fresh groundwater, driven by the oceanic oscillations, lead to the creation of subsurface estuary (subsurface analogue to surface estuary) as suggested by Moore [1999]. The role of a subsurface estuary in determining the terrestrial chemical input to the sea may be compared with that of a

surface estuary. Most previous studies of coastal groundwater, focusing on large-scale saltwater intrusion in aquifers, have ignored the dynamic effects of tides and waves on the flow and mixing processes in the near-shore area of the aquifer (e.g., Huyakorn *et al.* [1987]). Despite some early work on coastal groundwater flow and discharge to the sea [Cooper, 1959], it was not until the 1980s that researchers began to investigate the environmental and ecological impacts of groundwater discharge [Bokuniewicz, 1980; Johannes, 1980].

Globally, the fresh groundwater discharge has been estimated to be a few percent of the total freshwater discharge to the ocean [Zekster and Loaiciga, 1993]. Recently, Moore [1996] conducted experiments on ^{226}Radium enrichment in the coastal sea of the South Atlantic Bight. From the measurements, he inferred, on the basis of mass balance, that groundwater discharge amounts to as much as 40% of the total river flow into the ocean in the study area. This estimate contrasts with previous figures that range from 0.1 to 10%. Younger [1996] suggested that the recharge to the coastal aquifer could only support 4% of the estimated discharge. A model that includes recycling/exchanging water across the seabed was found to predict the excessive discharge rate [Li *et al.*, 1999].

Since the exchanging water is largely of marine origin, its impact on the fate of chemicals in the aquifer and chemical fluxes to coastal water depends on its mixing with groundwater. Laboratory experiments have revealed large tide-induced variations of flow velocities and salinity in the intertidal zone of the aquifer. This suggests that the mass transport of salinity is affected by tides significantly. The mixing of the tide-induced recycling water with fresh groundwater results in a salinity profile of two saline plumes near the shore [Boufadel, 2000], as schematically shown in Figure 1. The mixing zone is in contrast with the traditional saltwater wedge. Field measurements also showed fluctuations of salinity near the shore in response to tides and waves [Nielsen, 1999; Cartwright and Nielsen, 2001]. Tidal effects on salinity distribution in the aquifer have also been demonstrated by numerical investigations [Ataie-Ashtiani *et al.*, 1999; Zhang *et al.*, 2001]. These results suggest the existence of a mixing zone of the coastal aquifer that behaves much like an estuary. In this subsurface estuary, flow and mass transport/transformation are affected by both the net groundwater flow and water exchange/mixing induced by oceanic oscillations, particularly the tides.

The first part of the chapter is on the effects of tides on coastal groundwater, focusing on the water table fluctuations in shallow aquifers. Various analytical solutions of the tide-induced groundwater table fluctuations under different conditions will be presented briefly. The second

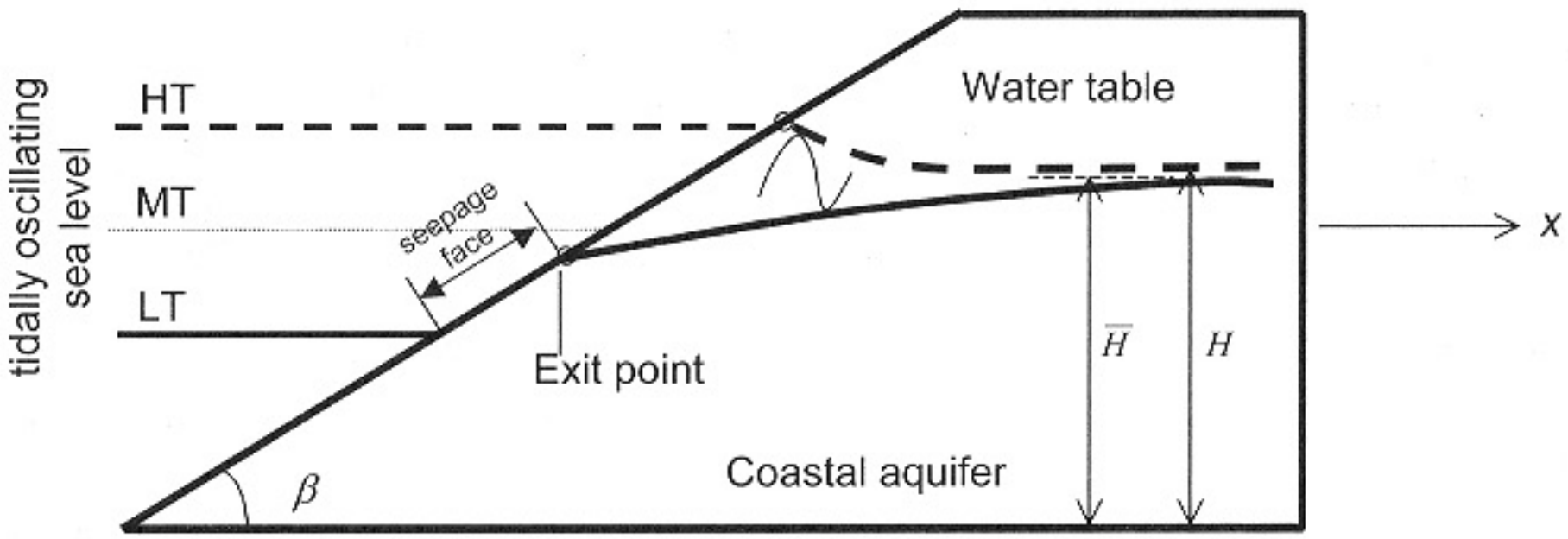

Figure 2: Schematic diagram of tidal conditions at the beach face and water table fluctuations in an unconfined aquifer.

part of the chapter is to examine the effects of the tide-induced groundwater fluctuations on the fate of chemicals in the near-shore aquifer and chemical fluxes to coastal waters. The discussion is based on several on-going studies aiming to improve the understanding and quantification of subsurface pathways and fluxes of chemicals to coastal environments. Additional materials of animated numerical simulation results and color plots are available on the accompanying CD.

2. TIDE-INDUCED GROUNDWATER OSCILLATIONS IN COASTAL AQUIFERS

Groundwater heads in coastal aquifers fluctuate in responses to oceanic tides. Such fluctuations have been subject to numerous recent studies (e.g., Nielsen [1990], Turner [1993], Li *et al.* [1997a], Nielsen *et al.* [1997], Baird *et al.* [1998], Raubenheimer *et al.* [1999], Li *et al.* [2000], Li and Jiao [2002a, b], Jeng *et al.* [2002]). In unconfined aquifers, such responses are manifested as water table fluctuations. These fluctuations are attenuated as they propagate inland, while the phases of the oscillations are shifted [Nielsen, 1990]. Modeling of tidal groundwater head fluctuations are often based on the Boussinesq equation assuming negligible vertical flow,

$$\frac{\partial h}{\partial t} = D\frac{\partial^2 h}{\partial x^2} \tag{1}$$

where h is the groundwater head fluctuation ($H - \overline{H}$, H is the total head and $\overline{H}$ is the mean head) as shown in Figure 2; x is the inland distance from the shore; t is time; and D is the hydraulic diffusivity, = T/S (S and T are the aquifer's storativity/specific yield and transmissivity, respectively). Note that Eq. (1) is a linearized Boussinesq equation. Although it is applicable to both confined and unconfined aquifers, the application to the latter requires that

the tidal amplitude be relatively small with respect to the mean aquifer thickness [Parlange *et al.*, 1984]. The effects of nonlinearity will be discussed later.

Analytical solutions for predicting tidal groundwater head fluctuations are available, for example [Nielsen, 1990],

$$h = A_0 \exp(-\kappa x)\cos(\omega t - \kappa x) \tag{2a}$$

where A_0 and ω are the tidal amplitude and frequency, respectively; κ is the rate of amplitude damping and phase shift, and is related to the tidal frequency and the aquifer's hydraulic diffusivity,

$$\kappa = \sqrt{\frac{\omega}{2D}} \tag{2b}$$

The solution can be presented in an alternative form,

$$h = \mathrm{Re}\left[A_0 \exp(i\omega t - kx)\right] \tag{3a}$$

with

$$\kappa = \sqrt{\frac{i\omega}{D}} \tag{3b}$$

where $i = \sqrt{-1}$ and k is the complex wave number. The relation expressed by Eq. (3b) is termed wave dispersion. The solution assumes that the seaward boundary condition of the groundwater head is defined by the tidal sea level oscillations, i.e.,

$$h(0,t) = A_0 \cos(\omega t) \tag{4}$$

Far inland ($x \to \infty$), the gradient of h is taken to be zero (the tidal effects are diminished), i.e.,

$$\left.\frac{\partial h}{\partial x}\right|_{x=+\infty} = 0 \tag{5}$$

This simple solution also assumes: $A_0/\bar{H}$ (for unconfined aquifers) small, i.e., negligible nonlinear effects; vertical beach face; negligible capillary effects; no leakage exchange between shallow and deep aquifers; negligible vertical flow effects ($\bar{H}\kappa$ small); and negligible seepage face formation. In the following, we discuss relevant effects in situations where these assumptions do not hold.

2.1 Nonlinear Effects

Parlange *et al.* [1984] examined the nonlinear effects. Their analysis is briefly presented here. The head fluctuation is governed by the nonlinear Boussinesq equation as follows,

$$\frac{\partial h}{\partial t} = \frac{K}{n_e}\frac{\partial}{\partial x}\left[\left(\bar{H} + h\right)\frac{\partial h}{\partial x}\right] \tag{6}$$

The seaward and landward boundary conditions are the same as described by Eqs. (4) and (5). A perturbation technique is applied to solve Eq. (6). The solution of h is sought for in the following form,

$$h = \bar{H}\left[\varepsilon h_1 + \varepsilon^2 h_2 + O\left(\varepsilon^3\right)\right] \tag{7}$$

where ε is the perturbation variable, = $A_0/\bar{H}$; it is less than unity under normal conditions. Substituting Eq. (7) into Eq. (6) results in two perturbation equations for h_1 and h_2. Solving these two equations gives,

$$h = A_0 \exp\left(-\kappa x\right)\cos\left(\omega t - \kappa x\right) +$$
$$\frac{A_0^2}{2\bar{H}}\left[\exp\left(-\sqrt{2}\kappa x\right)\cos\left(2\omega t - \sqrt{2}\kappa x\right) - \exp\left(-2\kappa x\right)\cos\left(2\omega t - 2\kappa x\right)\right] \tag{8}$$
$$+\frac{A_0^2}{4\bar{H}}\left[1 - \exp\left(-2\kappa x\right)\right]$$

The nonlinear effects as shown by Eq. (8) lead to the generation of a second harmonics (the second term of the right-hand side with frequency 2ω) and a water table overheight (increase of the mean water table height; the third term of the RHS). The superposition of the second harmonics and the primary signal gives rise to the asymmetry between the rising and falling phases of the water table fluctuations, often observed in the field.

2.2 Slope Effects

Nielsen [1990] reported the first analytical investigation on the slope effects. He derived a perturbation solution for small amplitude water table fluctuations based on the linearized Boussinesq equation by matching a prescribed series solution with the moving boundary condition due to the slope. Later, Li *et al.* [2000] presented an improved approach, as described below. To focus on the slope effects, only small amplitude tides are considered, as modeled by the linearized Boussinesq equation (1) subject to the boundary conditions defined by Eqs. (5) and (9).

As shown in Figure 3, tidal oscillations on a sloping beach create a moving boundary:

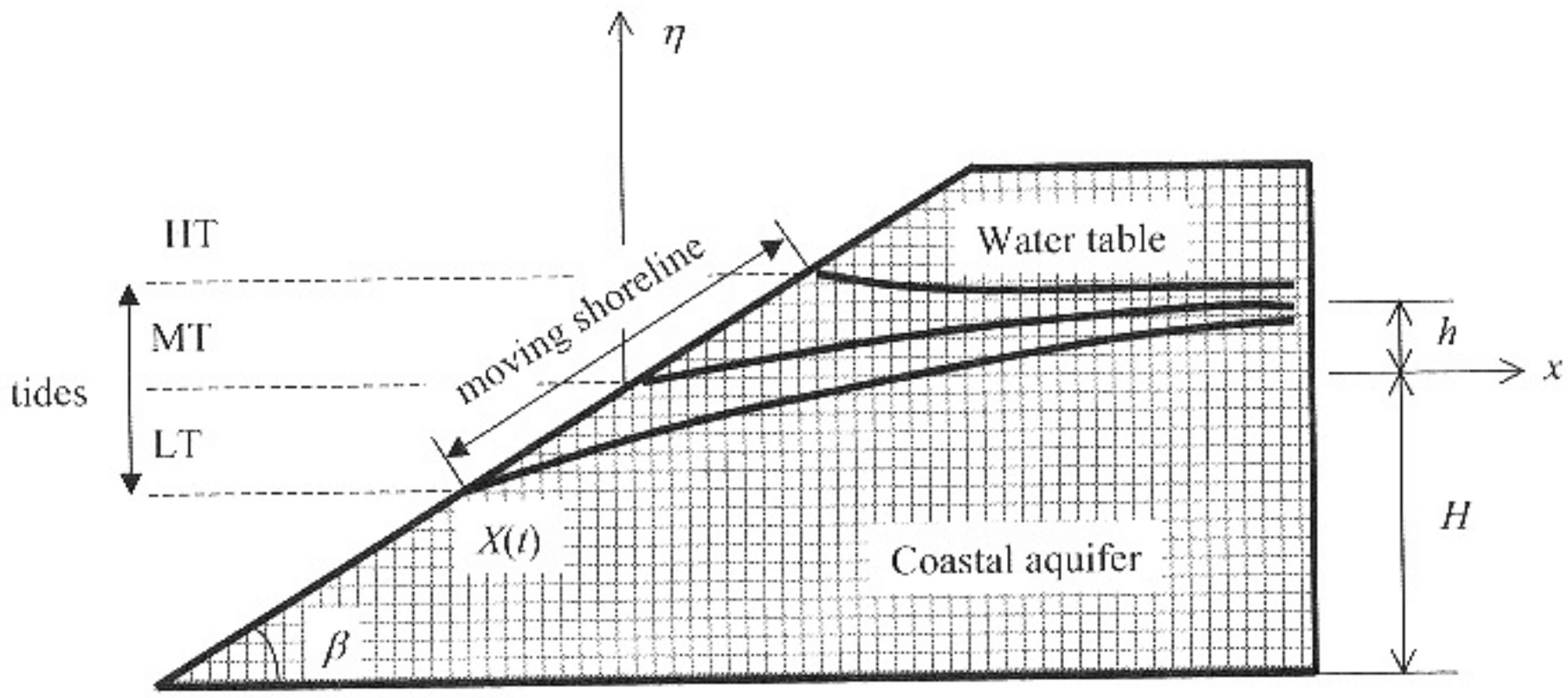

Figure 3: Schematic diagram of water table fluctuations in a coastal aquifer subject to tidal oscillations at the sloping beach face.

$$h\left[X(t),t\right]=\eta(t) \quad \text{and} \quad X(t)=\cot(\beta)\eta(t) \tag{9}$$

where $X(t)$ is the x-coordinate of the moving boundary (the origin of the x-coordinate is located at the intersection between the mid-tidal sea level and the beach face), β is the beach angle, and $\eta(t)$ represents tide-induced oscillations of the mean sea level. By introducing a new variable $z=x-X(t)$, Eqs. (1), (9) and (5) are, respectively, transformed to,

$$\frac{\partial h}{\partial t}=D\frac{\partial^2 h}{\partial z^2}-v(t)\frac{\partial h}{\partial z} \tag{10a}$$

$$h(0,t)=\eta(t) \tag{10b}$$

$$\left.\frac{\partial h}{\partial z}\right|_{z=+\infty}=0 \tag{10c}$$

where

$$v(t)=-\frac{dX(t)}{dt}=A\omega\cot(\beta)\sin(\omega t) \tag{10d}$$

The moving boundary problem of Eq. (1) is thus mapped to a fixed boundary problem of Eq. (10). A perturbation approach is adopted to solve Eq. (10), i.e.,

$$h=h_0+\varepsilon h_1+\mathrm{O}\left(\varepsilon^2\right) \tag{11}$$

where $\varepsilon=A\ \kappa\cot(\beta)$ and κ is given by Eq. (2b). The solution is,

$$h = A\exp(-\kappa z)\cos(\omega t - \kappa z) + \frac{A\varepsilon}{2}\left\{1+\sqrt{2}\exp\left(-\sqrt{2}\kappa z\right)\cos\left(2\omega t - \sqrt{2}\kappa z + \frac{\pi}{4}\right) - \sqrt{2}\exp(-\kappa z)\left[\cos\left(2\omega t - \kappa z + \frac{\pi}{4}\right) + \cos\left(\kappa z - \frac{\pi}{4}\right)\right]\right\} + O\left(\varepsilon^2\right) \tag{12}$$

To obtain the solution in the x-coordinate, one can substitute $z = x - A\cos(\beta)\cos(\omega t)$ into Eq. (12). The solution shows that the slope effects are qualitatively similar to those caused by the nonlinearity of finite amplitude tides, i.e., generation of the sub-harmonics and water table overheight.

2.3 Capillary Effects

Parlange and Brutsaert [1987] derived a modified Boussinesq equation to include the capillary effects,

$$\frac{\partial h}{\partial t} = \frac{K\bar{H}}{n_e}\frac{\partial^2 h}{\partial x^2} + \frac{B\bar{H}}{n_e}\frac{\partial^3 h}{\partial t\,\partial x^2} \tag{13}$$

where B is the average depth of water held in the capillary zone above the water table. Barry *et al.* [1996] solved this equation subject to the boundary conditions described by Eqs. (4) and (5),

$$h = A_0\exp(-\kappa_1 x)\cos(\omega t - \kappa_2 x) \tag{14a}$$

with

$$\kappa_1 = \sqrt{\frac{n_e\omega}{2\bar{H}}\left[\frac{1}{\sqrt{K^2+(\omega B)^2}} + \frac{\omega B}{K^2+(\omega B)^2}\right]} \tag{14b}$$

and

$$\kappa_2 = \sqrt{\frac{n_e\omega}{2\bar{H}}\left[\frac{1}{\sqrt{K^2+(\omega B)^2}} - \frac{\omega B}{K^2+(\omega B)^2}\right]} \tag{14c}$$

The capillary effects cause the difference between the damping rate (κ_1) and the wave number (κ_2). The solution suggests that capillary effects are only important for high frequency oscillations. Under normal conditions, the effects of unsaturated flows on the tidal water table fluctuations are small. More detailed discussion on the capillary effects can be found in Li *et al.* [1997b].

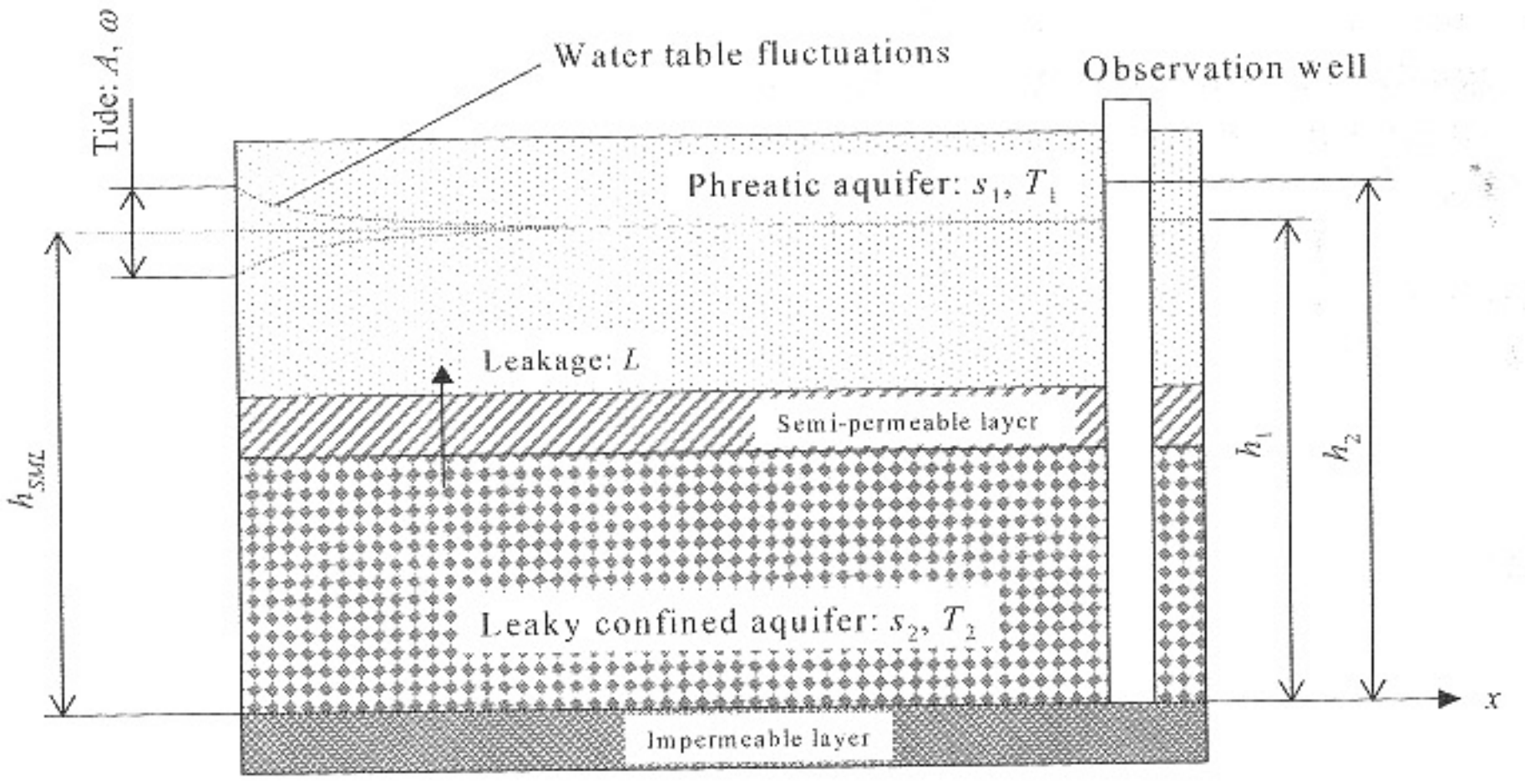

Figure 4: Schematic diagram of a leaky confined aquifer with an overlying phreatic aquifer.

2.4 Leakage Effects

In the above solutions, the bottom boundary of the aquifer is assumed to be impermeable. In reality, it is not uncommon to find composite aquifer systems such as the one shown in Figure 4: an unconfined aquifer overlying and separated from a confined aquifer by a thin semi-permeable layer. The groundwater heads fluctuate in both the confined and the phreatic aquifer. The two aquifers interact with each other via leakage through the semi-permeable layer [e.g., Bear, 1972]:

$$s_1 \frac{\partial h_1}{\partial t} = T_1 \frac{\partial^2 h_1}{\partial x^2} + L(h_2 - h_1) \tag{15a}$$

$$s_2 \frac{\partial h_2}{\partial t} = T_2 \frac{\partial^2 h_2}{\partial x^2} + L(h_1 - h_2) \tag{15b}$$

where h_1 and h_2 are the heads in the confined and the phreatic aquifers, respectively; T_1 and T_2 are the transmissivities of these two aquifers, respectively; s_1 is the specific yield of the phreatic aquifer and s_2 is the storativity of the confined aquifer; and L is the specific leakage of the semi-permeable layer.

In reality, the damping of the tidal signal in the unconfined aquifer is much higher than that in the confined aquifer (since $s_1 >> s_2$). Usually the fluctuations of h_1 become negligible 100 m landward of the shoreline while the tides propagate much further inland in the confined aquifer. Jiao and Tang [1999] solved Eq. (15b) assuming that h_1 is constant, i.e., neglecting

the tidal fluctuations in the unconfined aquifer. Their solution shown below suggests that the leakage reduces the tidal signal in the confined aquifer significantly, i.e., the damping rate increases:

$$h_2 = h_{MSL} + A_0 \exp(-k_{L1}x)\cos(\omega t - k_{L2}x) \tag{16a}$$

with

$$\kappa_{L1} = \sqrt{\frac{L}{2T_2} + \frac{1}{2}\sqrt{\left(\frac{\omega s_2}{T_2}\right)^2 + \left(\frac{L}{T}\right)^2}} \tag{16b}$$

and

$$\kappa_{L2} = \frac{\omega s_2}{2T_2\kappa_{L1}} \tag{16c}$$

Jeng *et al.* [2002] solved the coupled equations (15a) and (15b). Their solution also demonstrates the reduction of tidal signal in the confined aquifer due to leakage. However, the extent of the reduction is less than predicted by Eq. (16). The solution also indicates that the water table fluctuation in the unconfined aquifer is enhanced as a result of the leakage.

2.5 Low Frequency Oscillations

The above solutions consider only one tidal constituent. In reality, tides are more complicated and often bichromatic, containing oscillations of two slightly different frequencies: semi-diurnal solar tide with period $T_1 = 12$ h and frequency $\omega_1 = 0.5236$ Rad h^{-1}, and semi-diurnal lunar tide with $T_2 = 12.42$ h and $\omega_2 = 0.5059$ Rad h^{-1}. As a result, the spring-neap cycle (i.e., the tidal envelope) is formed with a longer period, $T_{sn} = 2\pi/(\omega_1 - \omega_2) = 14.78$ d. Raubenheimer *et al.* [1999] observed water table fluctuations of period T_{sn}. These fluctuations (called spring-neap tidal water table fluctuations, SNWTF) occurred much further inland than the primary tidal signals (diurnal and semi-diurnal tides). While one may relate this long period fluctuation to the spring-neap cycle, the cause of such a phenomenon is not readily apparent. Spring-neap tides are bichromatic signals as described by

$$\eta(t) = A_1 \cos(\omega_1 t) + A_2 \cos(\omega_2 t - \delta) \tag{17}$$

where A_1 and A_2 are the amplitude of the semi-diurnal solar and lunar tide, respectively, and δ is the phase difference between them. Only two primary forcing signals exist at the boundary. If they propagate in the aquifer independently (as would occur in a linearized model assuming a vertical beach face), the water table response will also be bichromatic and simply described by $A_1 \exp(-\kappa_1 x)\cos(\omega_1 t - \kappa_1 x) + A_2 \exp(-\kappa_2 x)\cos(\omega_2 t - \delta - \kappa_2 x)$.

Both κ_1 ($\sqrt{\frac{n_e\omega_1}{2KH}}$) and κ_2 ($\sqrt{\frac{n_e\omega_2}{2KH}}$) are high damping rates corresponding to the semi-diurnal frequencies. A slowly damped spring-neap tidal water table fluctuation is not predicted. However, the beach face is sloping and creates a moving boundary as discussed in Section 2.2. The moving boundary induces interactions between the two primary tidal signals as they propagate inland. Such interactions lead to the generation of the SNWTF.

Li *et al.* [2000] reported an analytical study on the SNWTF. The same approach as described in Section 2.2 was adopted to solve the Boussinesq equation subject to the bichromatic tides. The solution is as follows,

$$h = h_0 + \left(h_{10} + h_{11} + h_{12} + h_{13} + h_{14}\right)\varepsilon + \mathrm{O}\left(\varepsilon^2\right) \tag{18a}$$

$$h_0 = A_1 \exp\left(-\kappa_1 x\right)\cos\left(\omega_1 t - \kappa_1 x\right) + A_2 \exp\left(-\kappa_2 x\right)\cos\left(\omega_2 t - \kappa_2 x - \delta\right) \tag{18b}$$

$$h_{10} = \frac{1}{2}\left(A_1 + r_2\sqrt{r_1}A_2\right) \tag{18c}$$

$$h_{11} = \frac{\sqrt{2}A_1}{2}\exp\left(-\sqrt{2}\kappa_1 x\right)\cos\left(2\omega_1 t - \sqrt{2}\kappa_1 x + \frac{\pi}{4}\right) \tag{18d}$$

$$h_{12} = \frac{\sqrt{2}r_2\sqrt{r_1}A_2}{2}\exp\left(-\sqrt{2}\kappa_2 x\right)\cos\left(2\omega_2 t - \delta - \sqrt{2}\kappa_2 x + \frac{\pi}{4}\right) \tag{18e}$$

$$h_{13} = \frac{\sqrt{2}\left(1+\sqrt{r_1}\right)A_2}{2}\exp\left(-\kappa_3 x\right)\cos\left(\omega_3 t - \delta - \kappa_3 x + \frac{\pi}{4}\right) \tag{18f}$$

$$h_{14} = \frac{\sqrt{2r_1+2}A_2}{2}\exp\left(-\kappa_4 x\right)\cos\left(\omega_4 t - \delta - \kappa_4 x + \theta\right) \tag{18g}$$

where $\varepsilon = A_1\kappa_1\cot(\beta)$, $r_1 = \omega_2/\omega_1 = 0.9662$, $r_2 = A_2/A_1$, $\omega_3 = \omega_1 + \omega_2$, $\kappa_3 = \sqrt{1+r_1}\kappa_1$, $\omega_4 = \omega_1 - \omega_2$, $\kappa_4 = \sqrt{1-r_1}\kappa_1$ and $\theta = \arctan\left(\frac{1-\sqrt{r_1}}{1+\sqrt{r_1}}\right)$.

The solution indicates that, in a bichromatic tidal system, the moving boundary condition generates an overheight ($h_{10}\varepsilon$), and additional harmonic waves of frequency $2\omega_1$ ($h_{11}\varepsilon$), $2\omega_2$ ($h_{12}\varepsilon$), $\omega_1+\omega_2$ ($h_{13}\varepsilon$) and $\omega_1-\omega_2$ ($h_{14}\varepsilon$). The oscillation of $\omega_1-\omega_2$ represents the spring-neap tidal water table fluctuations. Since the damping rate, κ_4, is much smaller than κ_1, κ_2, and κ_3,

the SNWTF propagates much further inland, with a damping distance ($1/\kappa_4$) five times larger than those for the primary mode water table fluctuations.

2.6 Vertical Flow Effects (Intermediate Depth)

The validity of the Boussinesq equation depends on the shallowness of the aquifer, i.e., $n_e\omega\bar{H}/K$ small [Parlange *et al.*, 1984; Nielsen *et al.*, 1997]. For aquifers of intermediate depths, the vertical flow effects become considerable, in which case the Boussinesq equation needs to be expanded to include high-order terms, e.g., [Parlange *et al.*, 1984]

$$\frac{\partial h}{\partial t}=\frac{K}{n_e}\frac{\partial}{\partial x}\left[h\frac{\partial h}{\partial x}+h^2\frac{\partial h}{\partial x}\frac{\partial^3 h}{\partial x^2}+\frac{1}{3}h^3\frac{\partial^3 h}{\partial x^3}\right] \tag{19}$$

In a linearized form,

$$\frac{\partial h}{\partial t}=\frac{K\bar{H}}{n_e}\left[\frac{\partial^2 h}{\partial x^2}+\frac{\bar{H}^2}{3}\frac{\partial^4 h}{\partial x^4}\right] \tag{20}$$

The solution to Eq. (20) subject to the usual tidal boundary conditions is

$$h=A_0\exp\left(-\kappa_{v1}x\right)\cos\left(\omega t-\kappa_{v2}x\right) \tag{21a}$$

with

$$\kappa_{v1}=\mathrm{Re}\left(\frac{1}{\bar{H}}\sqrt{\frac{3}{2}}\sqrt{-1+\sqrt{1+\frac{4}{3}\frac{i\omega n_e\bar{H}}{K}}}\right) \tag{21b}$$

$$\kappa_{v2}=\mathrm{Im}\left(\frac{1}{\bar{H}}\sqrt{\frac{3}{2}}\sqrt{-1+\sqrt{1+\frac{4}{3}\frac{i\omega n_e\bar{H}}{K}}}\right) \tag{21c}$$

The behavior of κ_{v1} and κ_{v2} is different from that predicted by the Boussinesq solution. The vertical flow effects lead to difference between the damping rate and wave number (the rate of phase shift). In particular, the signal appears to propagate faster than predicted by the Boussinesq solution, i.e., smaller phase shifts.

Using a Rayleigh expansion of the hydraulic potential function in terms of the aquifer depth, Nielsen *et al.* [1997] derived a groundwater oscillation equation that includes an infinite number of high-order terms to account for the vertical flow effects.

2.7 Density Effects

The above solutions ignore the density effects due to seawater intrusion in the aquifer. Wang and Tsay [2001] investigated the density

effects based on a sharp interface approach and derived a governing equation for h including the density effects,

$$\frac{\partial h}{\partial t} = \frac{K}{n_e}\frac{\partial}{\partial x}\left[(\delta\eta + H)\frac{\partial h}{\partial x}\right] \tag{22}$$

where η is the height of the saltwater–freshwater interface from the base of the aquifer (H is the height of the water table also from the base of the aquifer) and δ is given by

$$\delta = \frac{\rho_s \nu_f}{\rho_f \nu_s} - 1 \tag{23}$$

where ρ_f and ρ_s are the density of the freshwater and seawater, respectively; and ν_f and ν_s are the kinematic viscosity of freshwater and seawater, respectively. Taking ρ_f = 1000 kg/m^3, ρ_s = 1020 kg/m^3, ν_f = 1.01 × 10^{-6} m^2/s, and ν_s = 1.06 × 10^{-6} m^2/s, δ is calculated to be –0.028. The ratio of $\delta\eta$ to H is at the maximum (near the shoreline where η is at the maximum, being close to H) –0.028. Equation (22) can therefore be approximated by the Boussinesq equation. In other words, the density effects on the water table fluctuations are negligible.

2.8 Seepage Face Effects

In reality, the occurrence of seepage faces is commonplace, in which case the exit point of the water table at the beach face is decoupled from the tidal signal (Figure 2). The boundary condition is then defined by the movement of the exit point rather than the tidal level. Based on the following model of Dracos [1963] and Turner [1993], one can show that the formation of seepage faces reduces the primary forcing signals (semi-diurnal solar and lunar tides) and causes a spring-neap forcing oscillation on the boundary. The inland propagation of this oscillation leads to the SNWTF too.

In the Turner/Dracos model, the movement of the exit point is described by,

Coupling phase:

$$z_e = z_s \quad \text{for} \quad V_{tide} \geq -\frac{K}{n_e}\sin^2(\beta) \tag{24a}$$

Decoupling phase:

$$z_e = z_{ep} - \frac{K}{n_e}\sin^2(\beta)(t - t_{ep}) \quad \text{for} \quad V_{tide} < -\frac{K}{n_e}\sin^2(\beta) \tag{24b}$$

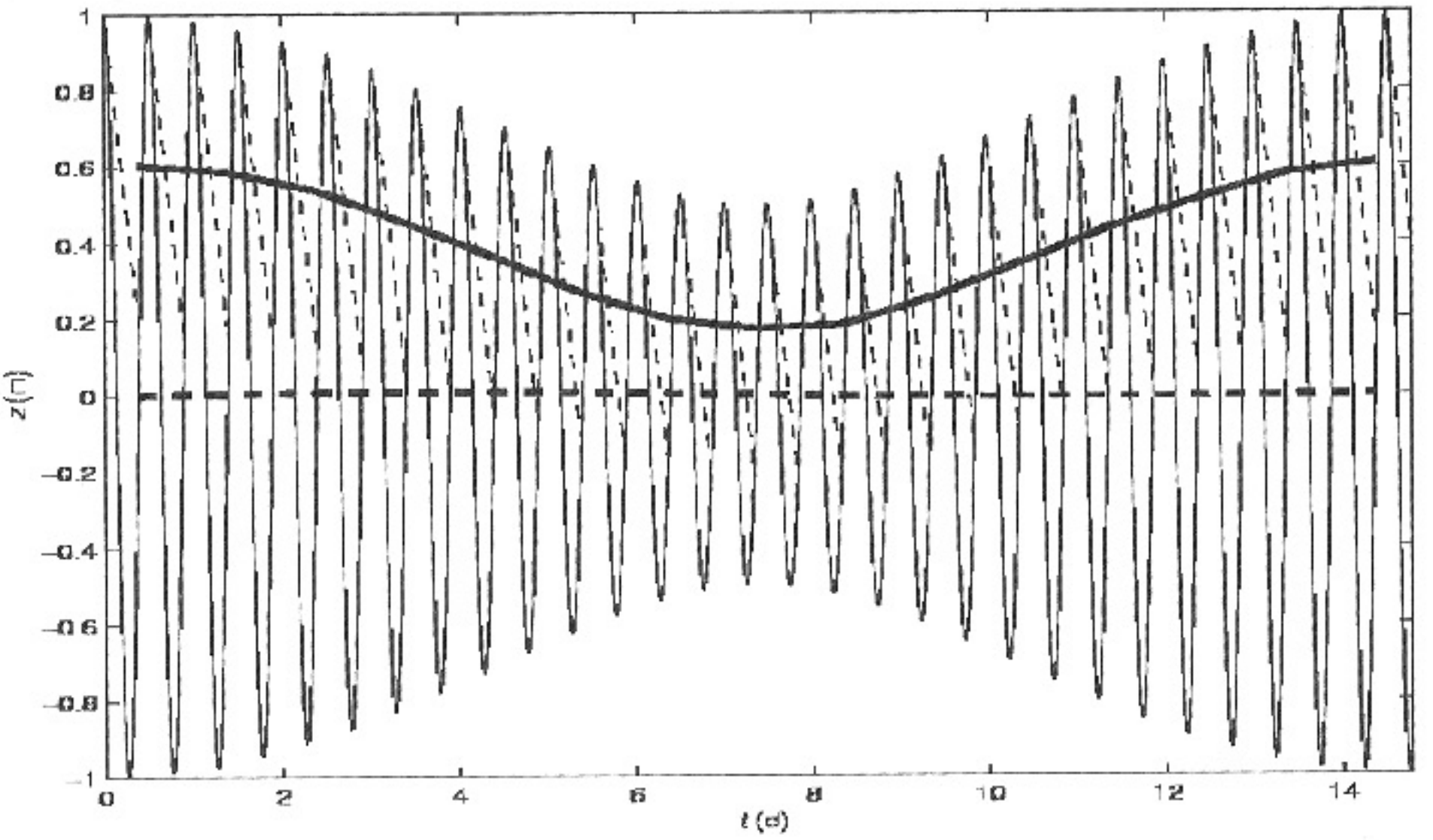

Figure 5: Calculated elevations of the sea level (thin solid line) and the exit point (thin dashed line). Thicker solid and dashed lines show the 25-h averaged elevations of the sea level and the exit point, respectively.

where z_e and z_s are the elevations of the exit point and shoreline, respectively; V_{tide} is the tidal velocity; t_{ep} is the instant when decoupling commences; and z_{ep} is the elevation of the exit point at time t_{ep}.

As an example, Figure 5 shows the calculated seepage face over a spring-neap cycle using the above model. The long period (of T_{sn}) oscillation is clearly evident in the exit point's movement. Further analysis based on the Fourier transformation shows that large oscillations occur at the spring-neap frequency while the amplitudes of the semi-diurnal oscillations are reduced by a factor of 0.4.

3. IMPLICATIONS FOR CONTAMINANT TRANSPORT AND TRANSFORMATION IN TIDALLY INFLUENCED COASTAL AQUIFERS

As demonstrated above, the tides affect significantly the coastal groundwater. The water table fluctuations are the manifestation of such effects in the shallow unconfined aquifer and have been studied extensively. These fluctuations result in oscillating groundwater flow in the near-shore area of the aquifer, enhancing the water exchange and mixing between the aquifer and coastal sea/estuary. In the following, we illustrate the importance

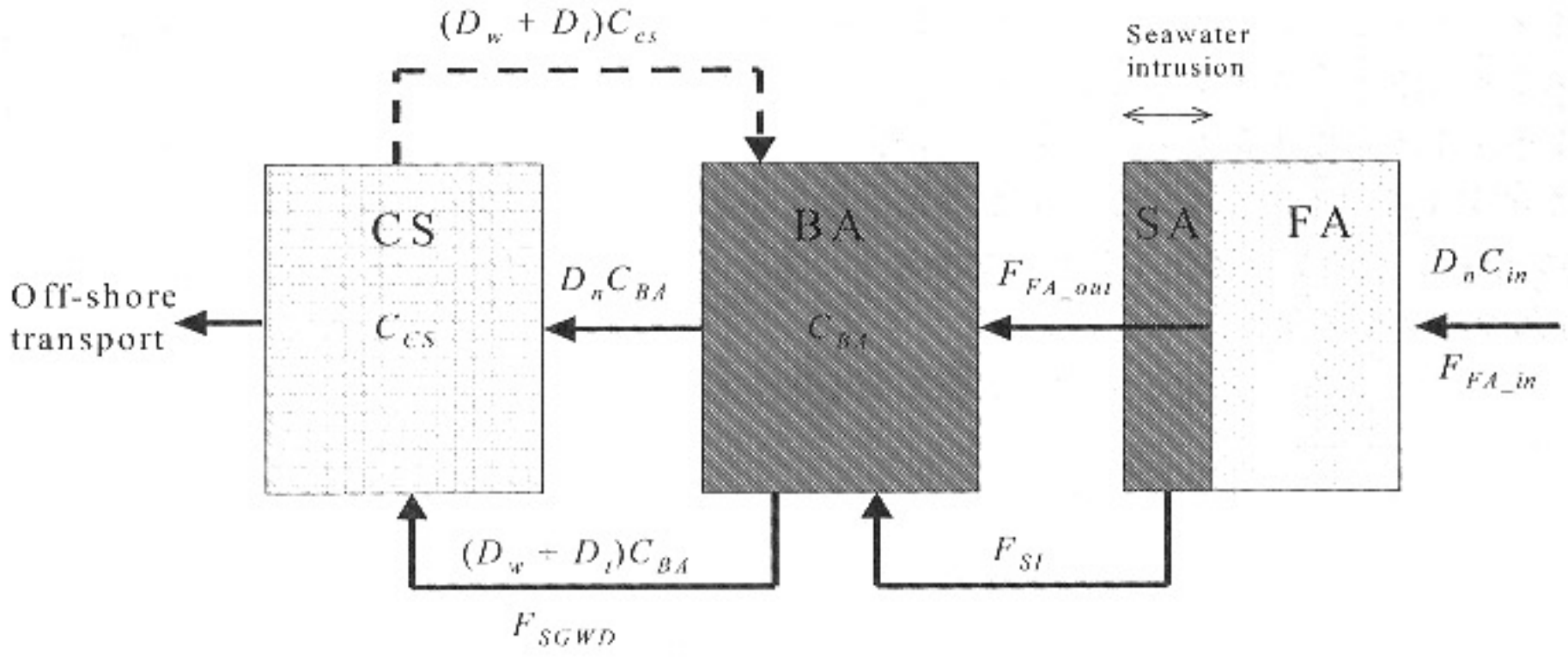

Figure 6: A box model of chemical transfer from the aquifer to coastal sea.

of these local flow, exchange, and mixing processes for chemical transport and transformation in the near-shore aquifer and the associated chemical fluxes to coastal water.

3.1 Tide-Induced Flushing and Dilution Effects on Chemical Transport Processes

Li *et al.* [1999] developed a model of SGWD that incorporates the outflows of the tide-induced oscillating groundwater flow and wave-induced groundwater circulation as well as the net groundwater discharge (Figure 1),

$$D_{SGWD} = D_n + D_w + D_t \tag{25}$$

Using a "box" model described below, Li *et al.* [1999] examined the importance of SGWD, especially D_w and D_t, on the process of chemical transfers from the aquifer to the ocean.

The model includes three water bodies: coastal sea (CS), brackish aquifer (BA), and freshwater aquifer (FA). Chemical transfers occur between the water bodies as shown by arrows in Figure 6. The chemicals are assumed to be strongly absorbed by sand particles in fresh groundwater and to desorb into brackish groundwater. The mass balance for FA can be described by

$$F_{FA\_in} = F_{FA\_out} \quad \text{if} \quad S = S_{eq} \tag{26a}$$

$$F_{FA\_out} = 0 \ \text{ and } \ V_{FA}\frac{dS}{dt} = F_{FA\_in} \quad \text{if } S < S_{eq}, \tag{26b}$$

$$F_{FA\_in} = D_n C_{in} \tag{26c}$$

$$S_{eq} = K_d C_{in} \tag{26d}$$

where F_{FA_in} and F_{FA_out} are the input and output mass flux for FA, respectively; S is the amount of absorbed chemical and the subscript eq denotes the equilibrium state; V_{FA} is the effective volume of the FA; K_d is the distribution coefficient; and C_{in} is the input chemical concentration. Equations (26a) and (26b) express the equilibrium and non-equilibrium states, respectively.

For BA, the governing equations are:

$$V_{BA}\frac{dC_{BA}}{dt} = \left(F_{FA\_out} + F_{SI} + F_{CS}\right) - F_{SGWD} \tag{27a}$$

$$F_{SGWD} = \left(D_n + D_w + D_t\right)C_{BA} \tag{27b}$$

$$F_{CS} = \left(D_n + D_w + D_t\right)C_{CS} \tag{27c}$$

$$F_{SI} = S\frac{dV_{SI}}{dt} \tag{27d}$$

where V_{BA} is the volume of BA and C_{BA} is the chemical concentration in BA. C_{CS} is the chemical concentration in the ocean and, for the contaminants considered, is usually small compared with C_{BA} and can be neglected. F_{SI} results from seawater intrusion. The chemical adsorbed on sand particles tends to desorb in seawater. Thus, seawater intrusion produces an input flux to BA, and the magnitude of this flux is related to the speed of seawater intrusion and the amount of adsorption S. V_{SI} is the volume of intruded seawater.

Chemicals such as phosphate and ammonia are, in most cases, land-derived pollutants as a result of nutrient leaching from the agricultural fertilizer. Sediments in the freshwater aquifer, as a temporary storage for these chemicals due to high adsorption, become the immediate source of chemicals to the brackish aquifer when seawater intrusion occurs and the chemicals desorb into the brackish groundwater from the sediment. Here, a simulation is presented to illustrate how the local groundwater circulation and oscillations affect the transfer of land-derived pollutants. In the simulation, the FA was assumed to be in an equilibrium state initially and seawater intrusion occurred between t = 0 and 10 d. The saltwater front retreated shoreward between t = 10 d and 20 d. Other assumptions were: K_d = 400. D_n = 3.75 m^3/d/m, $D_w + D_t$ = 90 m^3/d/m, $dV_s/dt = 5\%D_n$, C_{in} = 1 kg/m^3, and V_{BA} = 500 m^3/m. During seawater intrusion, the output mass flux from the FA is described by Eq. (26a) and during the retreat of the salt wedge, F_{FA_out} is given by Eq. (26b). The time that it takes for the FA to reach the equilibrium state after the retreat of the salt wedge can be estimated by $F_{SI}t_{SI}/F_{FA\_out}$.

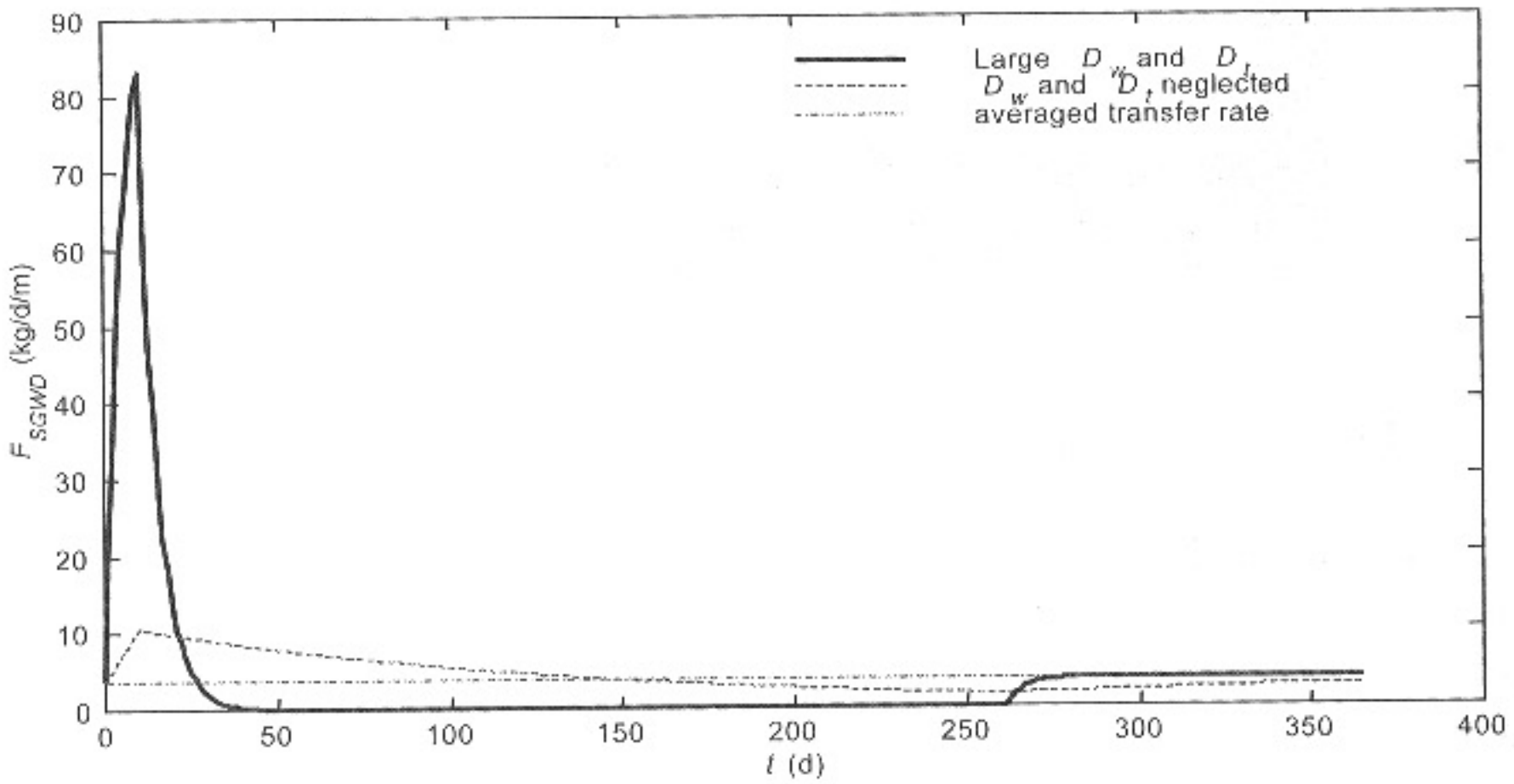

Figure 7: Simulated rates of the transfers of land-derived chemicals to the ocean.

The simulated rate of chemical transfer to the ocean is shown in Figure 7, with the results from a comparison simulation with D_n and D_t neglected. A large increase of the transfer rate is clearly evident as a result of the seawater intrusion and the local groundwater circulation/oscillating flows. The first factor (i.e., seawater intrusion) contributes to an extra and excessive source of the chemical. The second factor (i.e., the local groundwater circulation and oscillating flows) provides the mechanism for rapid flushing of the BA, resulting in increased chemical transfer to the ocean. Without the second factor, the large impulse of chemical input to the ocean would not occur as demonstrated by the comparison simulation (dashed curve in Figure 7). The increase of F_{SGWD} is substantial, more than 20 times as high as the averaged rate. As the salt wedge retreats, the transfer rate decreases to zero since the inland chemical is all adsorbed in the FA. The local processes do not change the total amount of the chemical input to the ocean, which is determined by the inland source.

The tide-induced flushing effect is further illustrated by the following simulation based on a one-dimensional mass transport model,

$$\frac{\partial c}{\partial t} = D_c \frac{\partial^2 c}{\partial x^2} - V \frac{\partial c}{\partial x} \tag{28a}$$

with

$$V = Ki_n + \sqrt{2} K \kappa A_0 \exp(-\kappa x) \cos\left(\omega t - \kappa x + \frac{\pi}{4}\right) \tag{28b}$$

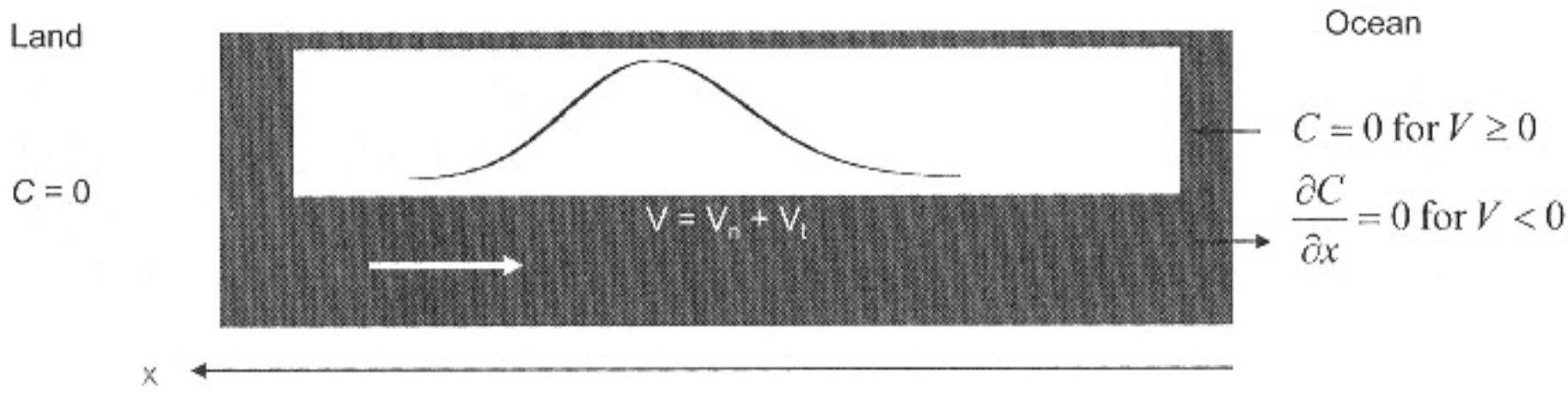

Figure 8: Tidal effects on transport of a contaminant plume.

The first term of the RHS of Eq. (28b) is the net groundwater flow rate and the second term represents the oscillating flow induced by tides (based on the analytical solution, Eq. (2)). The initial concentration is specified according to an existing plume shown in Figure 8. The boundary conditions for the chemical transport are: $c = 0$ at the inland boundary, and $c = 0$ for $V > 0$ and $\partial c/\partial x = 0$ for $V < 0$ at the seaward boundary. The following parameter values are used in the simulation: i_n (regional hydraulic gradient) = 0.01, A_0 = 0, 1 and 2 m, T (tidal period) = 0.5 d, K = 20 m/d, $\overline{H}$ = 10 m, n_e = 0.2, α = 3 m ($D_c = \alpha V$), L (distance of the landward boundary from the shore) = 150 m.

The results displayed in Figure 9 show that the residence time of the chemical in the aquifer decreases due to tidal oscillations (left-hand side panel of Figure 9). The tidal effects also lead to dilution of the exit chemical concentration significantly (right-hand side panel of Figure 9). Such dilution may reduce the impact of chemicals on the beach habitats.

3.2 Tide-Induced Mixing of Fresh Groundwater and Seawater

In this section, we address how the fresh groundwater discharges to the ocean. Previous studies, neglecting the tidal effects, predict that the freshwater overlies the intruded seawater and discharges to the ocean with little mixing with the saltwater. The limited mixing, driven by the density effects, occurs along the saltwater wedge. A simulation was conducted using SeaWat (http://water.usgs.gov/ogw/seawat/) to examine the tidal effects on the freshwater discharge. Density-dependent groundwater flow in a coastal aquifer subject to tidal oscillations was simulated with a set of parameter values representing the shallow aquifer conditions.

The simulation was run first without the tidal oscillations until a steady state was reached. The result of the salinity distribution in the aquifer shows the traditional view of the groundwater discharge as discussed above (top panel of Figure 10). The tide was then introduced into the simulation, which continued to run for 100 tidal cycles and reached a quasi-steady state. The result shows a very different salinity distribution from that without the tidal effects (middle panel of Figure 10). First, a saline plume was formed in

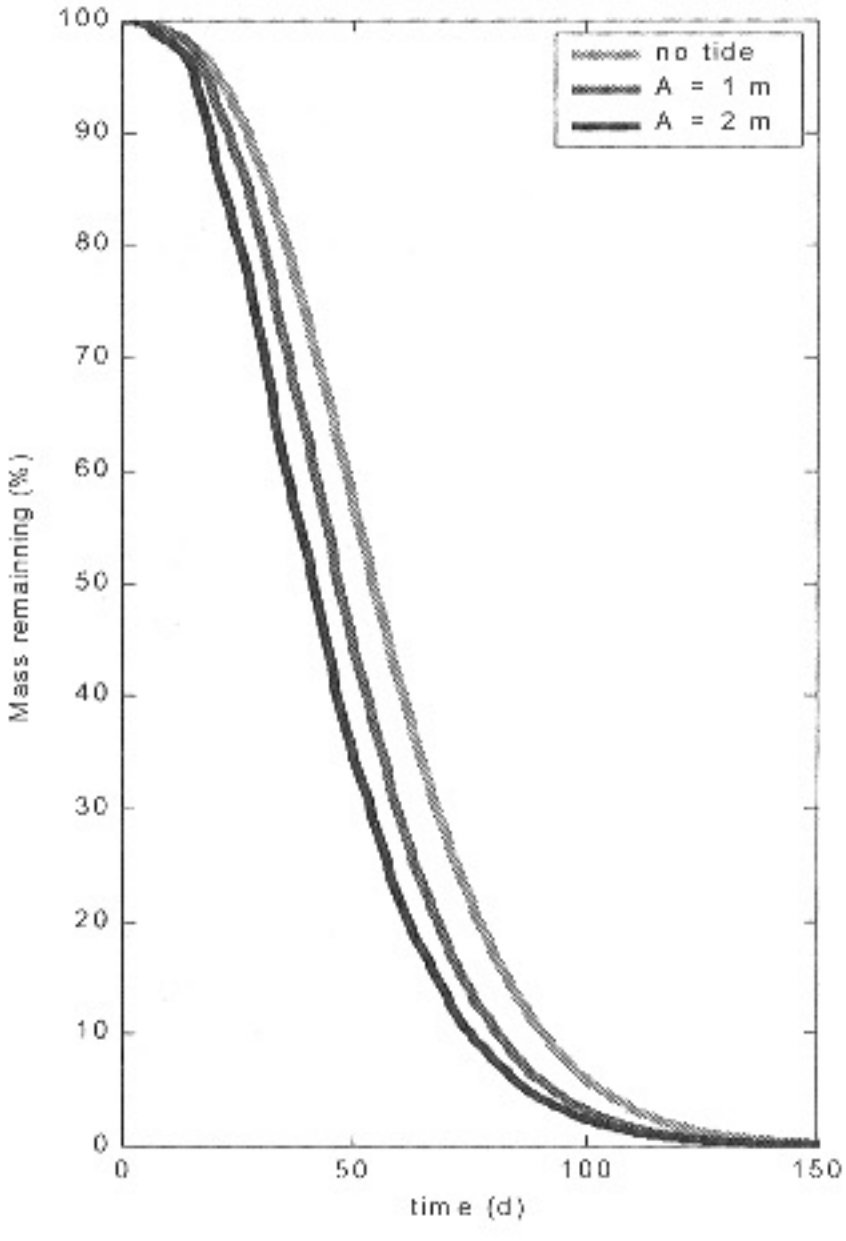

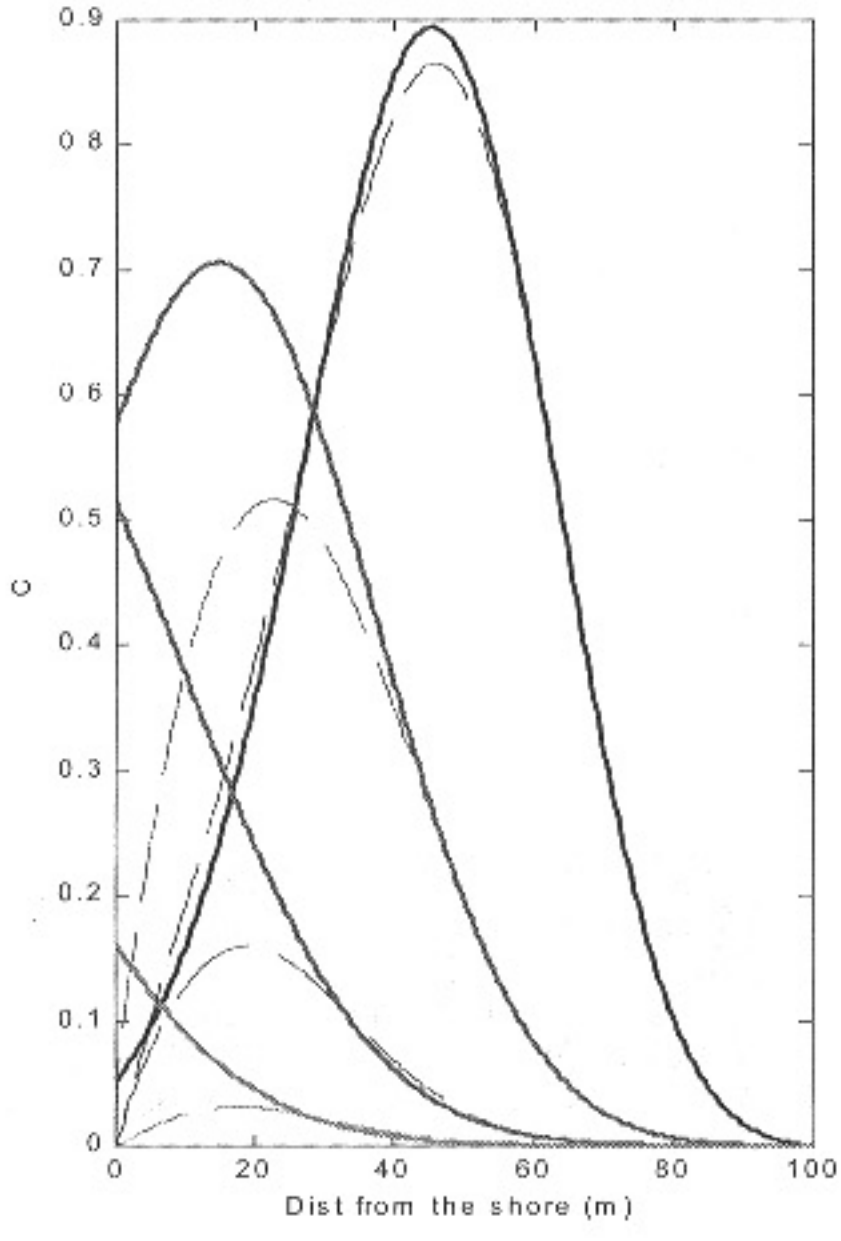

Figure 9: Tidal effects on chemical transport in a coastal aquifer. LHS panel: mass remaining in the aquifer (in percentage of the initial mass) versus time under different tidal conditions. RHS panel: chemical concentration profiles in the aquifer at different times (from the top to the bottom: the results shortly after the simulation started, a bit later, much later, and near the end of the simulation). Dashed lines are for results with tidal effects (A = 2 m) and solid lines for results without tidal effects.

the upper part of the beach. The freshwater discharged to the sea through a "tube" between this upper saline plume and the intruding saltwater wedge. Secondly, the freshwater discharge tube contracted and expanded as the tide rose and fell (shown in the attached animation), suggesting considerable mixing activities. Such mixing is also indicated by the salinity gradient shown in the bottom panel of Figure 10. These simulated salinity profiles are consistent with recent results from laboratory experiments [Boufadel, 2000].

In analyzing the simulated flow and mass transport process, we are particularly interested in (a) how the mean (advective) transport of salinity is affected by the oceanic oscillations, and (b) whether the oceanic oscillations (water exchange) cause diffusive/dispersive transport of salinity. This diffusive transport represents the local, small-scale mixing. For this purpose, the following decomposition is taken,

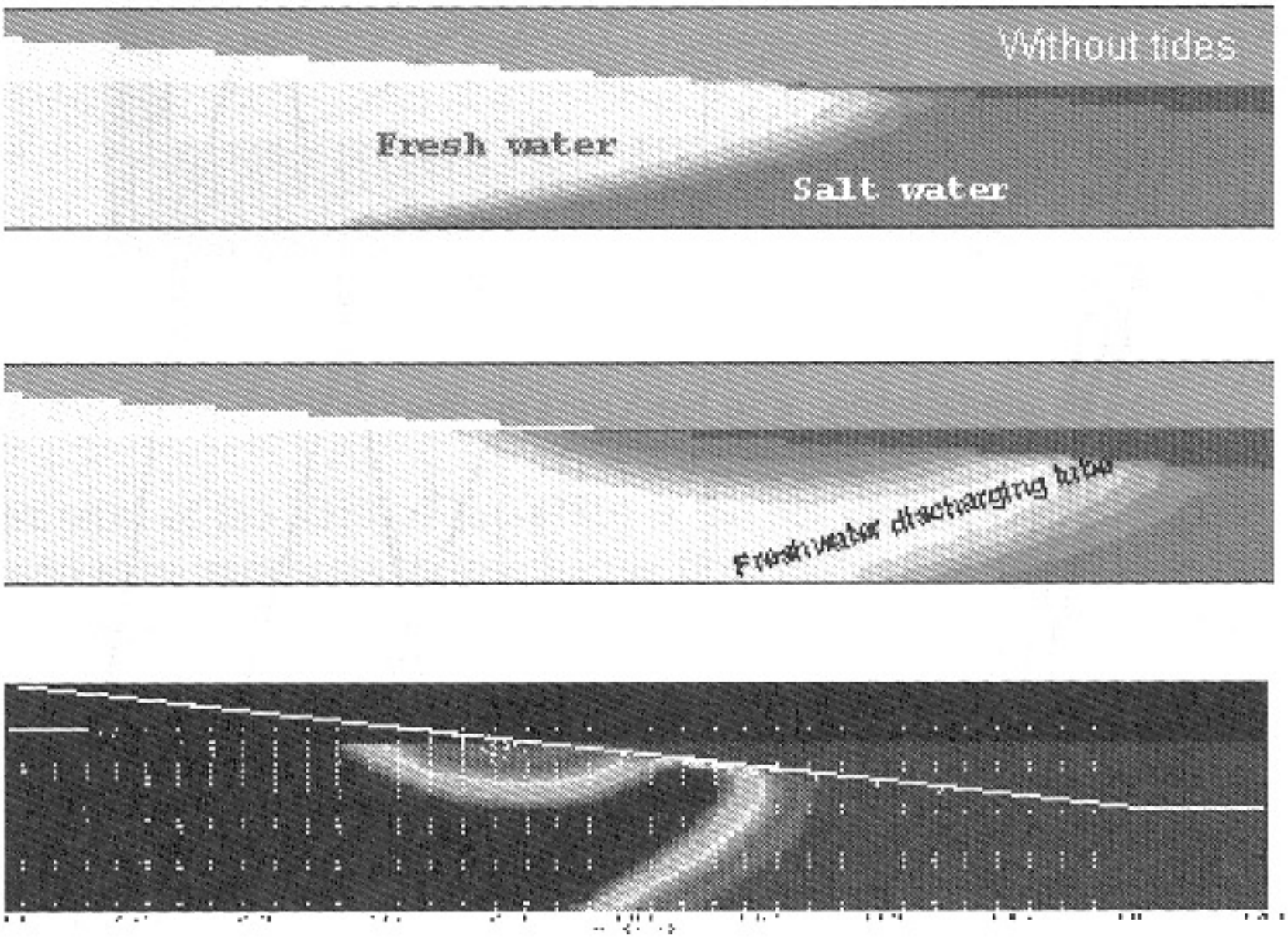

Figure 10: Salinity distribution in the near-shore area of the aquifer. Top panel: without tidal effects; fresh groundwater discharging to the sea without much mixing with underlying seawater. Middle panel: tidal effects leading to the formation of the upper saline plume and the freshwater discharging tube, and considerable mixing between the freshwater and seawater. Color plots are available on the CD.

$$u(x,z,t) = U(x,z) + u'(x,z,t) \tag{29a}$$

$$c(x,z,t) = C(x,z) + c'(x,z,t) \tag{29b}$$

where u and c are the raw data of instantaneous flow velocity and salinity; U and C are averaged flow velocity and salinity over the tidal cycle (24 hrs); and u' and c' are the tidally fluctuating flow velocity and salinity. The total mass transport of salinity can then be determined,

$$M = \overline{uc} = UC + \overline{u'c'} \tag{30}$$

The first term represents the transport due to the mean flow (advection). The second transport component is the diffusive/dispersive flux. In Figure 11, we show calculated mean transport flux and diffusive flux. It is interesting to note that the two fluxes exhibit quite different patterns, and the magnitude of

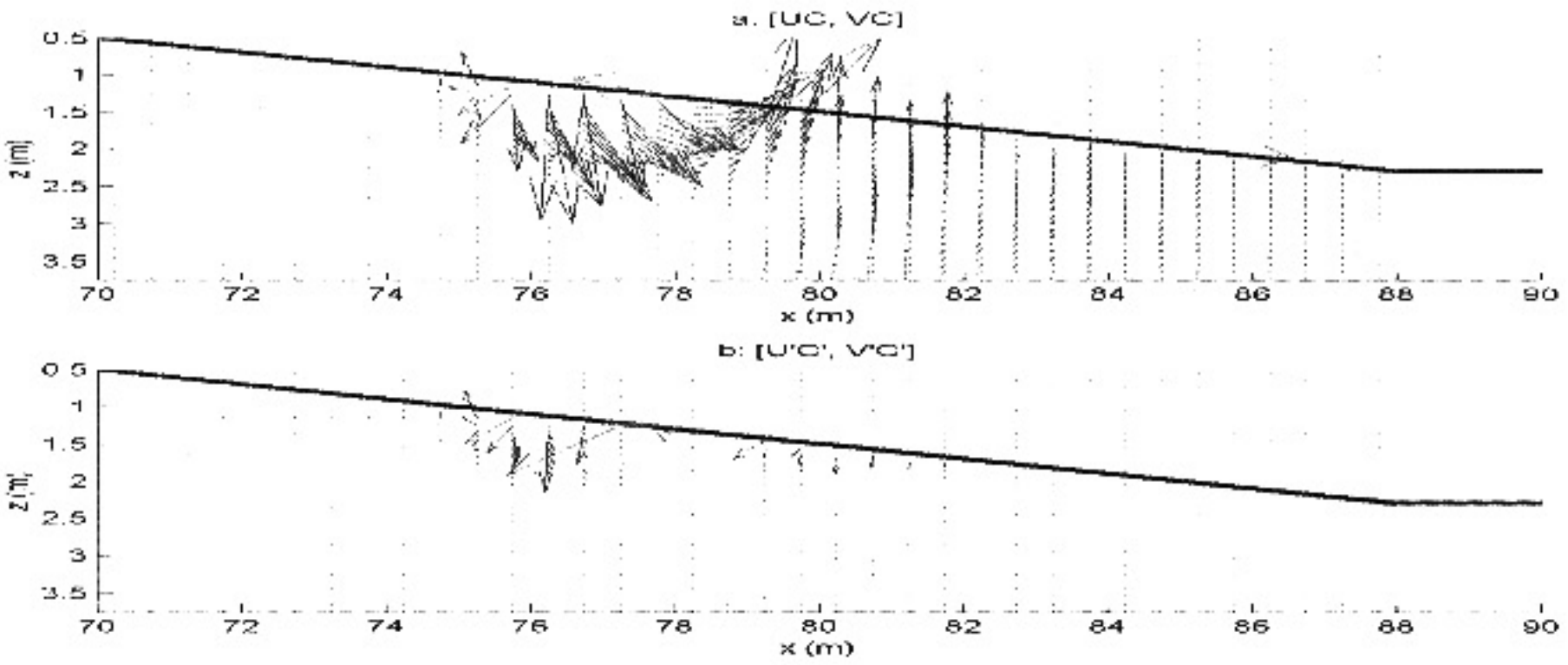

Figure 11: The mean (a) and diffusive (b) mass transport fluxes.

the mean transport flux is one order of magnitude larger than the diffusive flux. Based on the calculated diffusive/dispersive flux, one can estimate the apparent diffusion/dispersion coefficient (the local mixing intensity parameter),

$$D = \frac{\overline{u'c'}}{\nabla C} \tag{31}$$

where ∇C is the mean salinity gradient.

These results show that the tides affect the near-shore groundwater flow and transport processes significantly, leading to increased exchange and mixing between the aquifer and the ocean. Such effects can alter the geochemical conditions (redox state) in the aquifer and modify the chemical reactions. As shown numerically below, the exchange enhances the mixing of oxygen-rich seawater and groundwater, and creates an active zone for aerobic bacterial populations in the near-shore aquifer. This zone leads to a considerable reduction in breakthrough concentrations of aerobic biodegradable contaminants at the aquifer -ocean interface.

3.3 Tidal Effects on Chemical Reactions

MODFLOW and PHT3D were used to model contaminant transport and biodegradation in coastal aquifers affected by tidal oscillations. Two mobile chemicals were included in the simulation: oxygen as the electron acceptor and toluene as a representative biodegradable contaminant. An aerobic bacterium was included as an immobile phase. The biodegradation process was oxygen-limited (i.e., sufficient substrate). The inland contaminant source was specified at the cells near the water table (Figure 12).

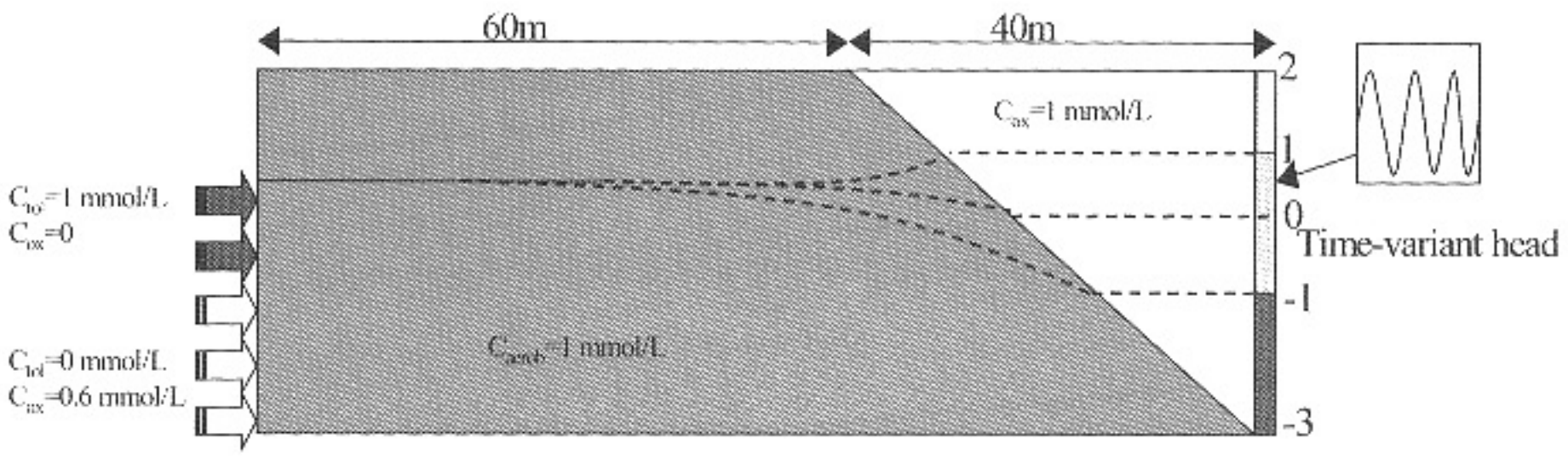

Figure 12: Schematic diagram of the model set-up and boundary conditions implemented in the simulation.

The simulation was run first without tides until a steady state of chemical concentrations was reached. Tides started after that. An animation of the simulation results is contained in the accompanying CD. The image plots of steady state concentrations for toluene, oxygen, and bacteria are shown in Figure 13. Due to the lack of oxygen, little degradation of toluene occurred except in the smearing diffusive layers. Correspondingly, little growth of bacteria can be observed. The chemical concentrations at a high tide after five tidal cycles were shown in Figure 14. The tidal effect is clearly evident: first it created an oxygen-rich zone near the shoreline, which led to biodegradation of toluene. Secondly, it enhanced the mixing process. The smearing layer was thickened. The results at the low tide show similar patterns and changes in the chemical concentrations. In short, the simulation demonstrates that tidal oscillations lead to the formation of an oxygen-rich zone in the near-shore aquifer area. Aerobic bacterial activity sustained by the high O_2 concentration in this active zone degrades the contaminants. These effects, largely ignored in previous studies, may have significant implications for the beach environment.

4. CONCLUSIONS

Coastal water pollution is a serious environmental problem around the world. Most contaminants are believed to be sourced from the land. To develop sound strategies for coastal water pollution control, we must be able to quantify the sources, pathways, and fluxes of contaminants to the coastal zone. Traditionally, terrestrial fluxes of chemicals to coastal water have been estimated on the basis of river flow alone. Recent studies suggest that contaminants entering the coastal zone with groundwater discharge can significantly contribute to coastal marine/estuarine pollution.

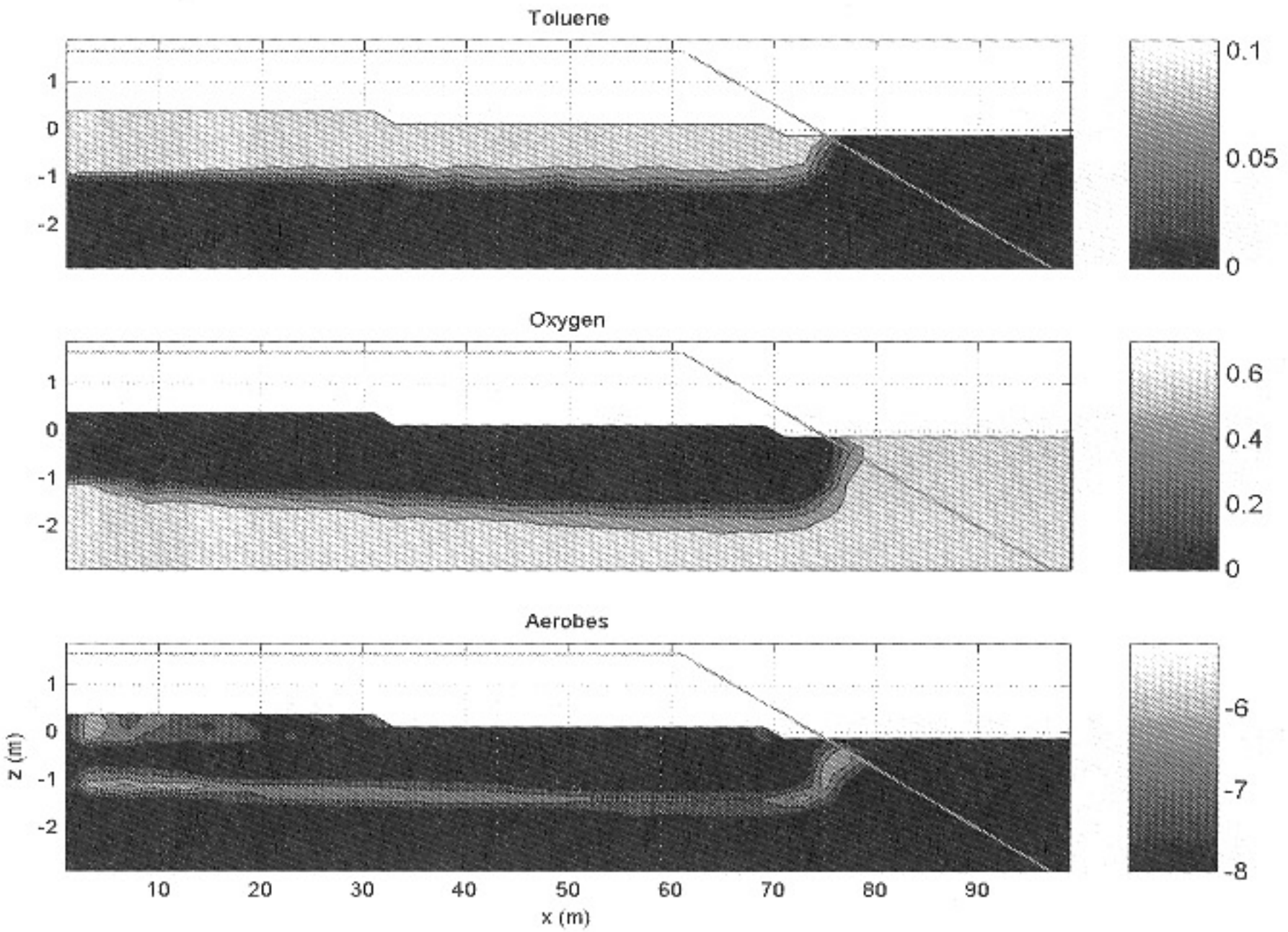

Figure 13: Image plots of the steady state concentrations for toluene (top panel), oxygen (middle panel), and bacteria (bottom panel). Color plots are available on the CD.

To determine the fluxes of chemicals to coastal water, it is important to quantify both the chemical transport processes and reactions on the pathway. There has been a large amount of research work conducted on how the chemicals may be transformed during the transport along the surface pathway, i.e., the role of a surface estuary. In contrast, little is known about the chemical transformation in the near-shore area of a coastal aquifer prior to chemicals' discharge to coastal water.

In this chapter, we first reviewed a large volume of work on tide-induced groundwater oscillations in coastal aquifers, focusing on analytical solutions of the tidal water table fluctuations. In the second part, we discussed the effects of tides and other oceanic oscillations on the chemical transport and transformation in the aquifer near the shore, drawing an analogy to the surface estuary–subsurface estuary. The discussion, based on several on-going studies, illustrated the important role that a subsurface estuary may play in determining the subsurface chemical fluxes to coastal waters. Although the tidal influence on the water table dynamics has been

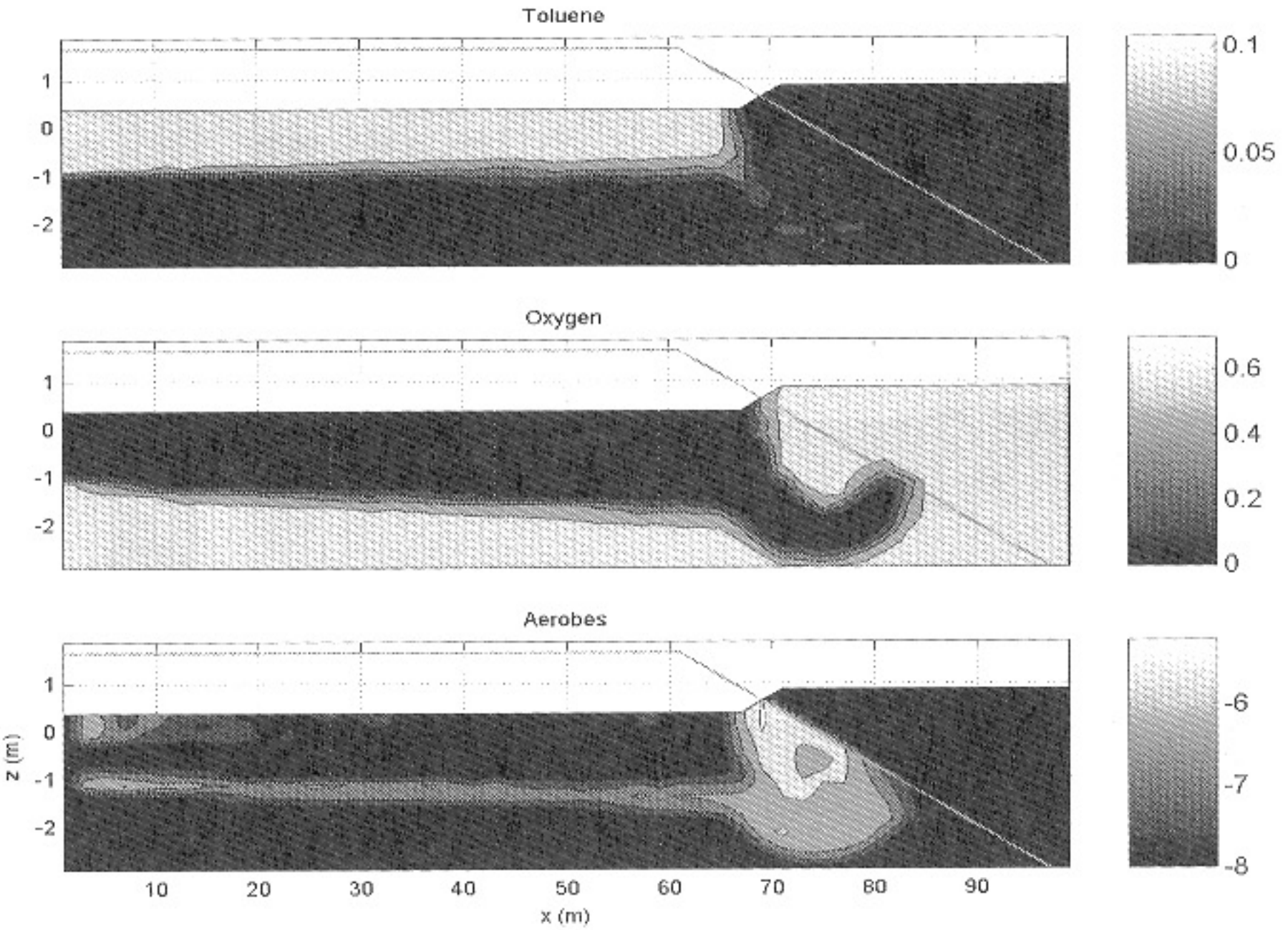

Figure 14: Image plots of the concentrations for toluene (top panel), oxygen (middle panel) and bacteria (bottom panel) at the high tide after five tidal cycles. Color plots are available on the CD.

subjected to numerous studies, the effects of tides on the fate of chemicals in the aquifer have not been investigated adequately. Quantification of these effects is clearly needed in order to

- provide better understanding of the pathway of land-derived nutrients and contaminants entering coastal waters; and
- provide useful information for integrating the management of upland and lowland catchments, and for improving strategies for sustainable coastal resources management and development.

Acknowledgments

Research work carried out by the authors on chemical transport and transformation in coastal aquifers was supported by the Leverhulme Trust (UK) under project F/00158/J.

REFERENCES

Ataie-Ashtiani, B., R.E. Volker, and D.A. Lockington, "Tidal effects on sea water intrusion in unconfined aquifers," *J. Hydrol.*, **216**, 17–31, 1999.

Baird, A.J., T. Mason, and D.P. Horn, "Validation of a Boussinesq model of beach groundwater behaviour," *Mar. Geol.*, **148**, 55–69, 1998.

Barry, D.A., S.J. Barry, and J.-Y. Parlange, "Capillarity correction to periodic solutions of the shallow flow approximation," In *Mixing Processes in Estuaries and Coastal Seas*, C. B. Pattiaratchi (ed.), AGU, Washington, DC, 496–510, 1996.

Bear, J., *Dynamics of Fluids in Porous Media*, Elsevier, New York, 1972.

Bokuniewicz, H., "Groundwater seepage into Great South Bay, New York," *Estuar. Coastal Mar. Sci.*, **10**, 437–444, 1980.

Boufadel, M.C., "A mechanistic study of nonlinear solute transport in a groundwater-surface water system under steady and transient hydraulic conditions," *Water Resour. Res.*, **36**, 2549–2565, 2000.

Buddemeier, R.W. (Ed.), *Groundwater discharge in the coastal zone*, LOICZ/R&S/96-8, Texel, The Netherlands, 1996.

Burnett, W.C., M. Taniguchi, and J. Oberdorfer, "Measurement and significance of the direct discharge of groundwater into the coastal zone," *J. Sea Res.*, 106–116, 2001.

Cartwright, N., and P. Nielsen, "Groundwater dynamics and salinity in coastal barriers," *Proc. 1st Int. Conf. Saltwater Intrusion &Coastal Aquifers*, D. Ouazar and A.H.-D. Cheng (eds.), April 23–25, Essaouira, Morocco, 2001.

Cooper, H.H., Jr., "A hypothesis concerning the dynamic balance of fresh water and salt water in a coastal aquifer," *J. Geophys. Res.*, **71**, 4785–4790, 1959.

Dracos T., Ebene nichtstationare Grundwasserabflusse mit freier Oberflache. Swiss Federal Technical Laboratory of Hydraulic Research and Soil Mechanics, *Rep. No. 57*, p. 114., 1963.

Enot, P., L. Li, H. Prommer, and D.A. Barry, "Effects of oceanic oscillations on aerobic biodegradation in coastal aquifers," *Geo. Res. Abs.*, European Geophysical Society, 3: 18, 2001.

Haynes, D., and K. Michael-Wagner, "Water quality in the Great Barrier Reef world heritage area: Past perspectives, current issues and new research directions," *Mar. Pollut. Bull.*, **41**, 7–12, 2000.

Huyakorn, P.S., P.F. Andersen, J.W. Mercer, and H.O. White, "Salt intrusion in aquifers: Development and testing of a three-dimensional finite element model," *Water Resour. Res.*, **23**, 293–319, 1987.

Jeng, D.S., L. Li, and D.A. Barry, "Analytical solution for tidal propagation in a coupled semi-confined/phreatic coastal aquifer," *Adv. Water Resour.*, **25**(5): 577–584, 2002.

Jiao, J.J., and Z.H. Tang, "An analytical solution of groundwater response to tidal fluctuation in a leaky confined aquifer," *Water Resour. Res.*, **35**, 747–751, 1999.

Johannes, R.E., "The ecological significance of the submarine discharge of groundwater," *Mar. Ecol. Prog. Ser.*, **3**, 365–373, 1980.

Li, H.L., and J.J. Jiao, "Analytical solutions of tidal groundwater flow in coastal two-aquifer system," *Adv. Water Resour.*, **25**, 417–426, 2002a.

Li, H.L., and J.J. Jiao, "Tidal groundwater level fluctuations in L-shaped leaky coastal aquifer system," *J. Hydrol.*, **268**, 234–243, 2002b.

Li, L., D.A. Barry, and C.B. Pattiarachi, "Numerical modelling of tide-induced beach water table fluctuations," *Coastal Eng.*, **30**, 105–123, 1997a.

Li, L., D.A. Barry, J.-Y. Parlange, and C.B. Pattiaratchi, "Beach water table fluctuations due to wave runup: Capillarity effects," *Water Resour. Res.*, **33**, 935–945, 1997b.

Li, L., D.A. Barry, F. Stagnitti, and J.-Y. Parlange, "Submarine groundwater discharge and associated chemical input to a coastal sea," *Water Resour. Res.*, **35**, 3253–3259, 1999.

Li, L., and D.A. Barry, "Wave-induced beach groundwater flow," *Adv. Water Resour.*, **23**, 325–337, 2000.

Li, L., D.A. Barry, F. Stagnitti, J.-Y. Parlange, and D.S. Jeng, "Beach water table fluctuations due to spring-neap tides," *Adv. Water Resour.*, **23**, 817–824, 2000.

Li, L., P. Enot, H. Prommer, F. Stagnitti, and D.A. Barry, "Effects of near-shore groundwater circulation on aerobic biodegradation in coastal unconfined aquifers," *Proc. 1st Int. Conf. Saltwater Intrusion & Coastal Aquifers*, D. Ouazar and A.H.-D. Cheng (eds.), April 23–25, Essaouira, Morocco, 2001.

Moore, W.S., "Large groundwater inputs to coastal waters revealed by ^{226}Ra enrichment," *Nature*, **380**, 612–614, 1996.

Moore, W.S., "The subterranean estuary: a reaction zone of ground water and sea water," *Mar. Chem.*, **65**, 111–125, 1999.

Nielsen, P., "Tidal dynamics of the water table in beaches," *Water Resour. Res.*, **26**, 2127–2134, 1990.

Nielsen, P., R. Aseervatham, J.D. Fenton, and P. Perrochet, "Groundwater waves in aquifers of intermediate depths," *Adv. Water Resour.*, **20**, 37–43, 1997.

Nielsen, P., "Groundwater dynamics and salinity in coastal barriers," *J. Coastal Res.*, **15**, 732–740, 1999.

Parlange J.-Y., F. Stagnitti, J.L. Starr, and R.D. Braddock, "Free-surface flow in porous media and periodic solution of the shallow-flow approximation," *J. Hydrol.*, **70**, 251–263, 1984.

Parlange, J.-Y., and W. Brutsaert, "A capillary correction for free surface flow of groundwater," *Water Resour. Res.*, **23**, 805–808, 1987.

Raubenheimer, B., R.T. Guza, and S. Elgar, "Tidal water table fluctuations in sandy beaches," *Water Resour. Res.*, **35**, 2313–2320, 1999.

Simmons, G.M., "Importance of submarine groundwater discharge and seawater cycling to material flux across sediment/water interfaces in marine environments," *Mar. Ecol. Prog. Ser.*, **84**, 173–184, 1992.

Turner, I., "Water table outcropping on macro-tidal beaches: A simulation model," *Mar. Geol.*, **115**, 227–238, 1993.

Turner, I.L, B.P. Coates, and R.I. Acworth, "Tides, waves, and super-elevation of groundwater at the coast," *J. Coastal Res.*, **13**, 46–60, 1997.

Wang, J. and T.-K. Tsay, "Tidal effects on groundwater motions," *Trans. Porous Media*, **43**, 159–178, 2001.

Younger, P.L., "Submarine groundwater discharge," *Nature*, **382**, 121–122, 1996.

Zekster, I.S., and H.A. Loaiciga, "Groundwater fluxes in the global hydrological cycle: past, present and future," *J. Hydrol.*, **144**, 405–427, 1993.

Zhang, Q., R. E. Volker, and D. A. Lockington, Influence of seaward boundary condition on contaminant transport in unconfined coastal aquifers, *J. Contam. Hydrol.*, **49**, 201–215, 2001.